The EMBO Journal (2008) 27, 3198–3208 | © 2008 European Molecular Biology Organization | Some Rights Reserved 0261-4189/08
www.embojournal.org

THE EMBO JOURNAL

EMBO open

Molecular basis for G-actin binding to RPEL motifs from the serum response factor coactivator MAL

Stephane Mouilleron[1,4], Sebastian Guettler[2,4,5], Carola A Langer[2], Richard Treisman[2,*] and Neil Q McDonald[1,3,*]

[1]Structural Biology Laboratory, Cancer Research UK, London Research Institute, London, UK, [2]Transcription Laboratory, Cancer Research UK, London Research Institute, London, UK and [3]School of Crystallography, Birkbeck College, London, UK

Serum response factor transcriptional activity is controlled through interactions with regulatory cofactors such as the coactivator MAL/MRTF-A (myocardin-related transcription factor A). MAL is itself regulated *in vivo* by changes in cellular actin dynamics, which alter its interaction with G-actin. The G-actin-sensing mechanism of MAL/MRTF-A resides in its N-terminal domain, which consists of three tandem RPEL repeats. We describe the first molecular insights into RPEL function obtained from structures of two independent RPEL^{MAL} peptide:G-actin complexes. Both RPEL peptides bind to the G-actin hydrophobic cleft and to subdomain 3. These RPEL^{MAL}:G-actin structures explain the sequence conservation defining the RPEL motif, including the invariant arginine. Characterisation of the RPEL^{MAL}:G-actin interaction by fluorescence anisotropy and cell reporter-based assays validates the significance of actin-binding residues for proper MAL localisation and regulation *in vivo*. We identify important differences in G-actin engagement between the two RPEL^{MAL} structures. Comparison with other actin-binding proteins reveals an unexpected similarity to the vitamin-D-binding protein, extending the G-actin-binding protein repertoire.

The EMBO Journal (2008) **27,** 3198–3208. doi:10.1038/emboj.2008.235; Published online 13 November 2008
Subject Categories: chromatin & transcription; structural biology
Keywords: actin; MAL; RPEL; SRF; structure

*Corresponding authors. R Treisman, Transcription Laboratories, Cancer Research UK, London Research Institute, 44 Lincoln's Inn Fields, London WC2A 3PX, UK. Tel.: +44 207 269 3727; Fax: +44 207 269 3093; E-mail: richard.treisman@cancer.org.uk or NQ McDonald, Structural Biology Laboratory, Cancer Research UK, London Research Institute, 44 Lincoln's Inn Fields, London WC2A 3PX, UK. Tel.: +44 207 269 3259; Fax: +44 207 269 3258; E-mail: neil.mcdonald@cancer.org.uk
[4]These authors contributed equally to this work
[5]Present address: Samuel Lunenfeld Research Institute, Mount Sinai Hospital, 600 University Avenue, Toronto, Canada M5G 1X5

Received: 6 August 2008; accepted: 10 October 2008; published online: 13 November 2008

Introduction

Actin is a major cytoskeletal constituent that can polymerise to form helical actin filaments (F-actin), the organisation of which contributes to cellular mechanical strength. Regulated assembly, rearrangement and disassembly of F-actin are critical in a wide variety of cellular processes, including cell morphology, cell motility and cellular interactions required for tissue formation and integrity (reviewed by Geiger and Bershadsky, 2001; Revenu *et al*, 2004; Chhabra and Higgs, 2007). Actin also participates in non-cytoskeletal processes, including transcription and chromatin remodelling, but here its functional roles and the molecular interactions involved are only poorly understood (Miralles and Visa, 2006; Chen and Shen, 2007; Su *et al*, 2007). One such system is actin-mediated control of the myocardin family transcriptional coactivators MAL/MRTF-A (myocardin-related transcription factor A) and MKL2/MRTF-B, which transduce Rho GTPase signals to the transcription factor serum response factor (SRF) (Cen *et al*, 2003; Miralles *et al*, 2003). Binding of unpolymerised actin (G-actin) to the MRTF N terminus inhibits MRTF activity by preventing their nuclear accumulation and repressing transcriptional activation by the MRTF–SRF complex (Miralles *et al*, 2003; Posern *et al*, 2004; Vartiainen *et al*, 2007).

The MRTF regulatory domain contains three copies of the RPEL motif (core sequence RPxxxEL; Pfam accession number: PF02755) (Finn *et al*, 2006), each of which functions as an actin-binding element (Guettler *et al*, 2008). Mutations at invariant positions within each RPEL motif impair interaction with G-actin and de-repress the activity of the MRTF proteins (Miralles *et al*, 2003; Vartiainen *et al*, 2007; Guettler *et al*, 2008). Similarly, myocardin, the constitutively nuclear and active founding member of the myocardin family to which the MRTFs belong (Wang *et al*, 2001), has a greatly reduced affinity for actin, reflecting sequence variations in its RPEL motifs (Guettler *et al*, 2008). These observations have led to the proposal that MRTF relocalisation and activation are regulated directly by actin through RhoA-induced alterations in the availability of G-actin (Miralles *et al*, 2003; Vartiainen *et al*, 2007; Guettler *et al*, 2008). RPEL motifs also mediate G-actin binding by members of the Phactr/Scapinin family of phosphatase-1-binding proteins, but here their functional significance is unknown (Sagara *et al*, 2003; Allen *et al*, 2004).

The actin monomer comprises four subdomains: in the actin filament, subdomains 1 and 3 are exposed at the barbed end, whereas subdomains 2 and 4 are exposed at the pointed actin filament end. F-actin assembly is regulated by actin concentration, by ATP hydrolysis and by interactions

between actin and regulatory proteins that control filament nucleation, polymerisation, severing or maintenance of the G-actin pool itself (reviewed by Pollard, 2007). A common feature in many G-actin-binding proteins is an amphipathic helix that engages a hydrophobic cleft separating actin subdomains 1 and 3, an interaction which is also likely to occur between actin protomers in F-actin (Holmes *et al*, 1990; Dominguez, 2004; Chereau *et al*, 2005).

The molecular basis for the RPEL^{MAL}:G-actin interaction, and how this relates to sequence conservation within the motif, were unknown. MAL:actin interaction interferes with F-actin assembly (Posern *et al*, 2004). MAL:actin binding is disrupted by profilin, swinholide A, jasplakinolide, cytochalasin D and tetramethylrhodamine actin modification, but is compatible with LatB and DNase I binding (Posern *et al*, 2004; SG, unpublished observations). Taken together with previous structural studies of actin interactions (Kabsch *et al*, 1990; Schutt *et al*, 1993; Morton *et al*, 2000; Otterbein *et al*, 2001; Klenchin *et al*, 2005), these data suggest that interaction between the RPEL motifs and actin is likely to involve the subdomain 1–3 hydrophobic cleft. However, the RPEL motif shares no obvious sequence similarities with other cleft-binding domains such as the WH2/verprolin domains (Dominguez, 2004). Here, we present crystal structures of two RPEL peptides from MAL individually bound to G-actin. Each RPEL peptide presents two consecutive helices that bind actin in a similar manner to two non-contiguous helices in the vitamin-D-binding protein (DBP):G-actin complex. This observation draws attention to four conserved positions shared by most G-actin cleft-binding proteins. Structural and biophysical data combined with cell-based reporter assays show that the sequence conservation that defines the RPEL motif reflects its activity as an actin-binding element crucial to the regulation of MAL *in vivo*.

Results

For our structural analyses, we assembled purified skeletal muscle G-actin bound to latrunculin B (LatB) and ATP with individual 32-residue RPEL peptides from murine MAL. These peptides corresponded to RPEL1^{MAL}, RPEL2^{MAL} and RPEL3^{MAL} and are known to bind actin efficiently *in vitro* (Guettler *et al*, 2008). High-resolution structures of the RPEL1^{MAL}:LatB–actin:ATP and RPEL2^{MAL}:LatB–actin:ATP complexes (hereafter shortened to RPEL^{MAL}:G-actin complexes) were subsequently determined and refined, but we were unable to crystallise the RPEL3^{MAL}:G-actin complex (Supplementary Table 1). When bound to actin, RPEL1^{MAL} and RPEL2^{MAL} each contain two helices (α1 and α2) connected by a short loop and end with a short C-terminal capping (C-cap) region (Ermolenko *et al*, 2002) (Figure 1A). The observed helical contents of RPEL1^{MAL} and RPEL2^{MAL} are consistent with secondary structure predictions (56, 65 and 47%, respectively, for each of the three MAL RPEL peptides). However, circular dichroism (CD) experiments revealed that each RPEL peptide is largely unstructured in solution (α-helical content of 5.2, 4 and 4.3%, respectively) (Supplementary Figure S1), indicating that the observed RPEL peptide secondary structure is induced on binding actin.

Structure of the RPEL2^{MAL}:G-actin complex

We first describe the higher resolution RPEL2^{MAL}:G-actin structure as it has a canonical RPEL sequence as defined in the Pfam database (Figure 1A). RPEL2^{MAL} wraps around actin, making intimate contacts with the subdomain 1–3 hydrophobic cleft and a ledge on subdomain 3 (Figure 1B). A total surface area of 1070 A^2 is buried within the interface, accounting for almost 30% of the RPEL2 surface area and 60% of RPEL2 residues. Helix α1^{RPEL2} (residues 115–123) binds within the actin hydrophobic cleft in a similar manner to WH2-containing proteins that engage this region (Figure 1B; Dominguez, 2004). α1^{RPEL2} runs from front to back in the standard view of actin (Figure 1B), making hydrophobic contacts through residues L118, I122 and the aliphatic portion of K121 to the base of the actin subdomain 1–3 hydrophobic cleft (Figure 1C). The Nε of K121 adopts two conformations, one hydrogen bonding with the G146^{actin} main chain carbonyl oxygen and the other forming a salt bridge with the side chain of E167^{actin}.

The invariant arginine, R125 in RPEL2^{MAL}, is located within the short loop (defined hereafter as the R-loop) connecting the helices α1^{RPEL2} and α2^{RPEL2} (Figures 1B and 2A). The R125 side chain, which is critical for actin interaction (Guettler *et al*, 2008), forms a cation–π interaction with the Y169^{actin} side chain through its guanidino group, as well as a side chain hydrogen bond with the main chain carbonyl oxygen of E167^{actin} (Figure 1C). Furthermore, R125 makes a salt bridge with the C-terminal carboxylate of F375^{actin}, the C-terminal residue of actin. The four residues within the R-loop have an extended conformation. The conserved proline, P126, constrains the R-loop backbone and stabilises the acute angle between α1^{RPEL2} and α2^{RPEL2}. Its carbonyl oxygen, together with the R128 main chain nitrogen, hydrogen bond with the Y169^{actin} hydroxyl moiety (Figure 1C). Y169^{actin} therefore has a central and crucial function to RPEL2 interaction having its side chain anchored through R-loop hydrogen bonds and pincered between the R125 side chain and those from R128/L131 (see below) (Figure 2B, right panel).

Helix α2^{RPEL2} (residues 128–134) and its C-cap residues 135–137 contact a 'ledge' on actin subdomain 3 centred on Y166^{actin}. The only other actin-binding protein shown to engage this region of actin in a similar manner is the structurally unrelated DBP (Otterbein *et al*, 2002; Verboven *et al*, 2003) (see Discussion section). Contacts with the subdomain 3 ledge are predominantly hydrophobic involving RPEL2 side chains L131, I136 and L137 (Figure 1C; Supplementary Figure S2B, right panel). Overall, the RPEL2^{MAL}:G-actin structure reveals that the majority of RPEL motif sequence conservation occurs at positions that mediate direct interactions with actin (Figure 2A) or intra-RPEL molecular interactions within the actin complex. The RPEL motif thus reflects the preservation of a functional G-actin-binding element.

Distinct differences in RPEL1^{MAL} and RPEL2^{MAL} R-loop actin contacts

The RPEL1^{MAL}:G-actin structure shares many of the interactions seen in the RPEL2^{MAL}:G-actin complex. These are made by structurally equivalent hydrophobic residues in helix α1 (residues 72–79), helix α2 (residues 84–92) and the C-cap (Supplementary Figure S2A and B). The RPEL1^{MAL} interac-

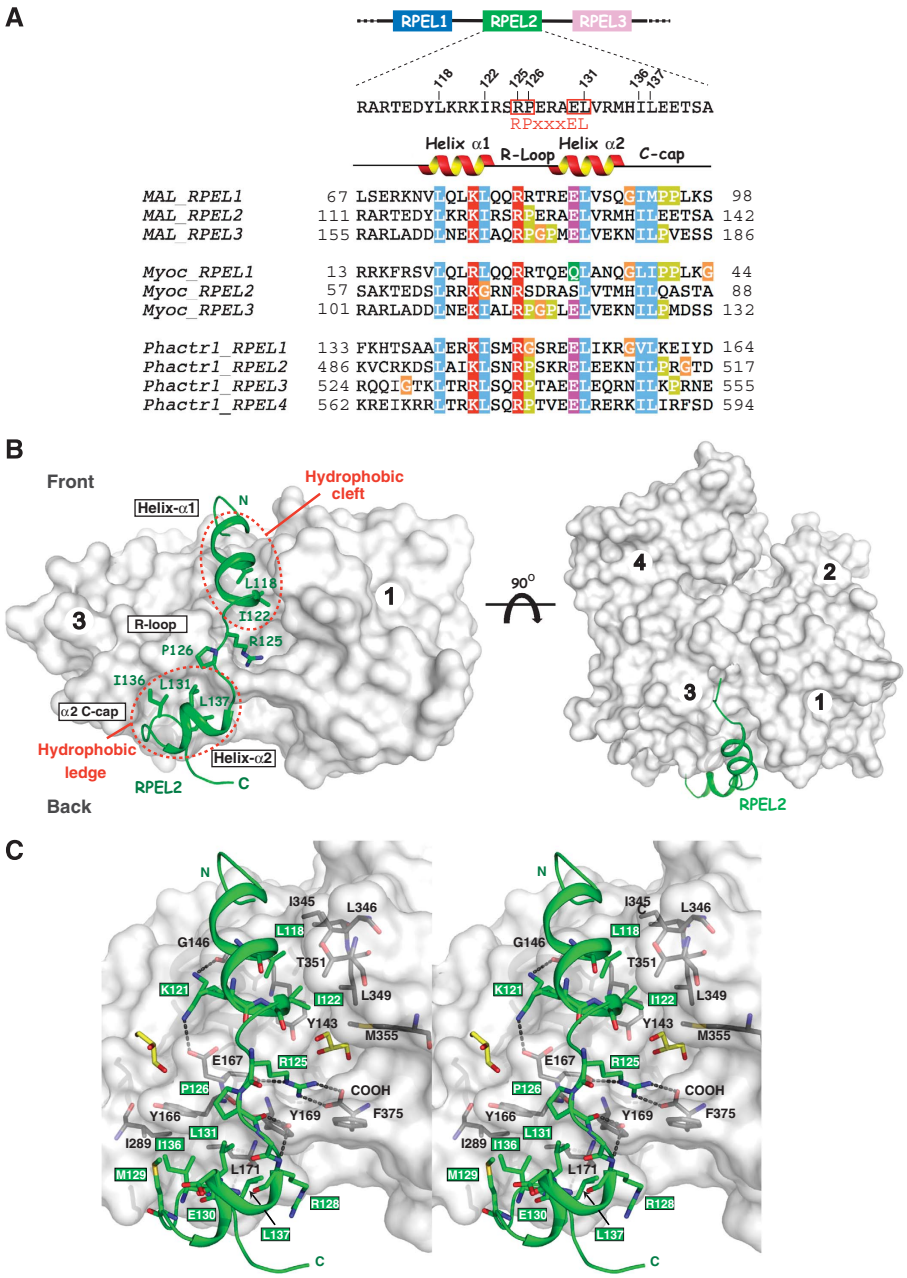

Figure 1 Structure of an RPEL peptide bound to G-actin. (**A**) Sequence alignment of individual RPEL motifs from murine MAL, myocardin (transcript variant A) and Phactr1. RPEL2^{MAL} secondary structure and features discussed in text are shown above the sequence. Selected conserved residues are highlighted. (**B**) Two views of the RPEL2^{MAL}:G-actin complex, related by a 90° rotation around the horizontal axis. Right-hand panel is the classical view of the 'front' surface of actin (white with subdomains labelled 1–4). RPEL2^{MAL} is drawn in green (cartoon) with highly conserved RPEL residues that interact with actin shown as sticks. The hydrophobic cleft and the subdomain 3 ledge of actin are indicated by red dashed circles. (**C**) Stereo view of the RPEL2^{MAL} (green cartoon) interaction with G-actin. Actin surface is drawn as per (B) with selected RPEL-interacting residues shown as grey sticks and key hydrogen bonds are indicated as dashed lines. Two glycerol molecules, used as a cryoprotectant, are shown in yellow.

tion surface with actin is slightly smaller than for RPEL2^{MAL} (811 Å^2) despite the higher affinity (see below). Core contacts from the R-loop R81 side chain and R84 main chain, which stack either side of Y169, are preserved (Figure 2B). However, there are significant differences in the way R-loop^{RPEL1} contacts actin, mainly reflecting its non-canonical R**R**xxxEL core sequence (Figure 1A). The R-loop^{RPEL1} follows a trajectory distinct from R-loop^{RPEL2} with an r.m.s. difference of 2.9 Å over 12 C-alpha atoms (calculated by superposing only their respective actin partners), indicating a degree of structural plasticity (Figure 2C). This difference most likely reflects the substitution of the canonical RPEL proline by R82, which makes RPEL1-specific actin contacts, specifically a salt bridge with E167^{actin} and a hydrogen bond with the phenolic oxygen of Y166^{actin} (Figure 2C; Supplementary Figure S2A). These contacts draw the RPEL1^{MAL} peptide away from Y169^{actin} such that the C-alpha atom of invariant R81^{RPEL1} is 3.0 Å from the equivalent R125 of RPEL2 (Figure 2B and C). R-loop main chain hydrogen bond distances to the Y169^{actin} side chain are therefore much longer in RPEL1^{MAL}. Strikingly, R81 is unable

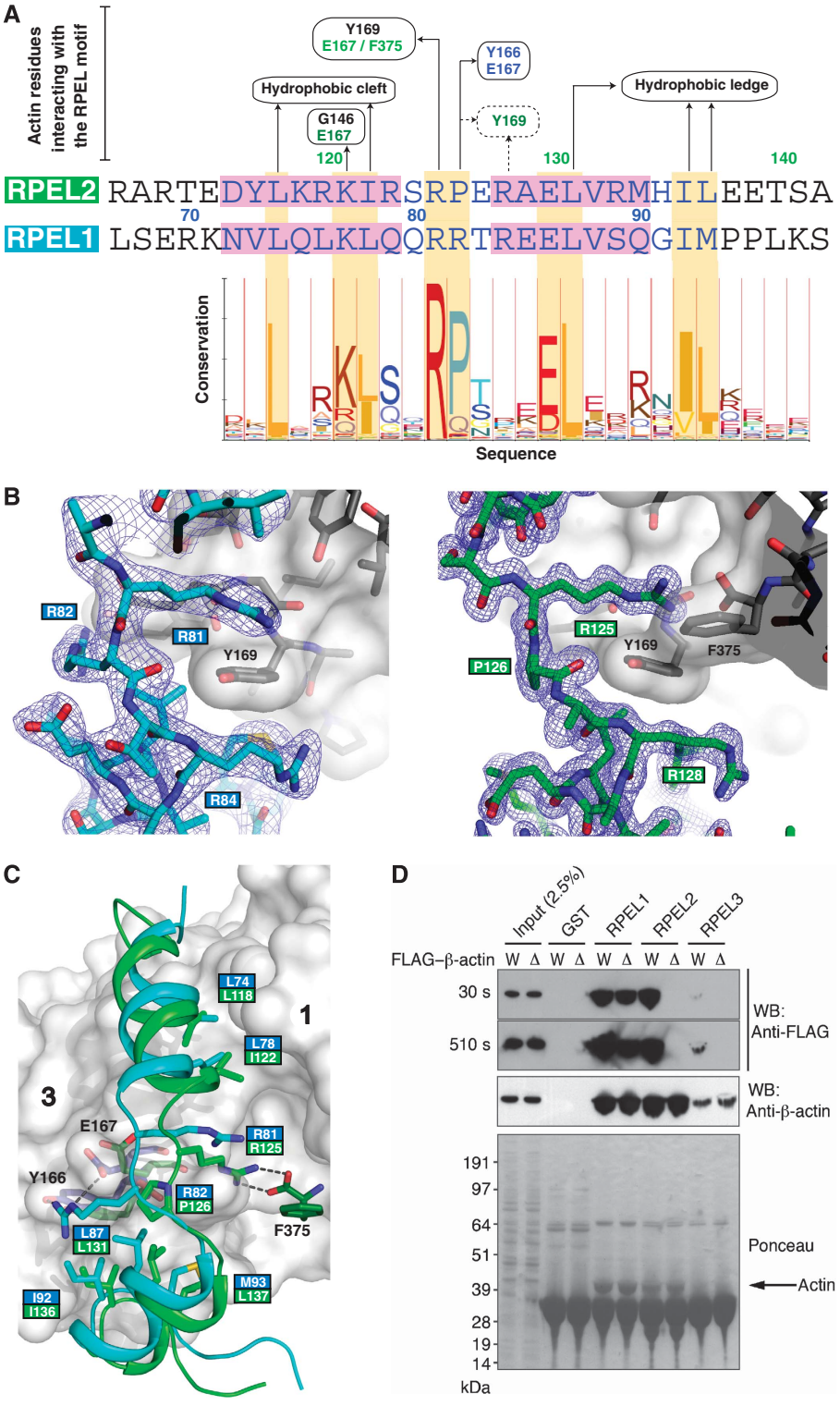

Figure 2 The RPEL1^{MAL} and RPEL2^{MAL} R-loops make different contacts with G-actin. (**A**) Summary of RPEL1/RPEL2 interactions with G-actin mapped onto a HMM (Hidden Markov Model) representation for the RPEL motif (Schuster-Bockler *et al*, 2004). Helices α1 and α2 are highlighted in pink and conserved residues from the RPEL HMM are highlighted in yellow. Boxes with solid lines indicate RPEL^{MAL} side chain-mediated interactions with actin, whereas those with dashed lines describe RPEL^{MAL} main chain-mediated interactions. Interactions that are conserved between RPEL peptides 1 and 2 are shown in black text and RPEL1- and RPEL2-specific ones in blue and green, respectively. (**B**) Close-up view of RPEL1^{MAL} and RPEL2^{MAL} interactions close to Y169^{actin}. Left panel, RPEL1^{MAL}:G-actin; right panel, RPEL2^{MAL}:G-actin. A $2mF_o-DF_c$ electron density map calculated around each RPEL is shown in blue contoured at 1 σ. Note that F375 is disordered in the RPEL1:actin complex. (**C**) Comparison of RPEL1^{MAL} (cyan) and RPEL2^{MAL} (green) motifs following superposition of their respective actin subunits. Important RPEL and G-actin residues described in the text are highlighted. Selected actin residues are shown in dark blue (contacting RPEL1) and dark green (contacting RPEL2), respectively. (**D**) Loss of F375 of β-actin affects binding of MAL RPEL motifs differentially. NIH3T3 fibroblasts transiently expressing either wild-type FLAG–β-actin (W) or FLAG–β-actin-ΔF375 (Δ) lacking the C-terminal residue were lysed and extracts were probed with bacterially produced GST or GST–RPEL peptide fusions as indicated. NIH3T3 cell lysates (input) and bound material were subjected to SDS–PAGE and western blotting for detection of the FLAG tag (WB: anti-FLAG) or endogenous β-actin (WB: anti-β-actin). Ponceau stain of the membrane indicates the levels of GST fusion proteins.

to reach and form a salt bridge with the C-terminal carboxylate of F375^{actin}, which is instead disordered (Figure 2B; Supplementary Figure S2A). To the best of our knowledge, only the twinfilin C-terminal domain has been shown earlier to make contact with the carboxylate of F375$^{G\text{-}actin}$ (Paavilainen *et al*, 2008).

To validate these apparent differences in how RPEL1^{MAL} and RPEL2^{MAL} engage actin, we tested whether complex formation by RPEL1^{MAL} and RPEL2^{MAL} is differentially sensitive to deletion of F375^{actin} using GST–RPEL pull-down assays (Guettler *et al*, 2008). RPEL1^{MAL} and RPEL2^{MAL} recovered exogenous wild-type β-actin and endogenous β-actin efficiently from total cell lysates, but only the RPEL2^{MAL}:G-actin interaction was sensitive to deletion of F375^{actin}, in agreement with our structural data (Figure 2D). RPEL3^{MAL} was also sensitive to the F375^{actin} deletion, despite its much lower apparent affinity for G-actin (Figure 2D), and would thus be predicted to bind in a similar manner to RPEL2^{MAL}.

Fluorescence anisotropy validation of MAL RPEL:G-actin interaction

To confirm the structural features of each RPEL^{MAL}:G-actin interaction, we performed fluorescence anisotropy assays using N-terminally FITC-conjugated RPEL peptides analogous to those used for the structural studies. Peptides were incubated with LatB-bound G-actin (peptide 0.5 μM; LatB–actin 0–59 μM) and the actin-binding affinity was calculated from anisotropy by nonlinear regression. The results are shown in Figure 3A. We also included an analysis of MAL RPEL3, for which no structural data are available. The wild-type peptides corresponding to RPEL1 and 2 bound relatively tightly, with apparent dissociation constants (K_d) of 1.0 ± 0.3 and 1.9 ± 0.1 μM, respectively, whereas the RPEL3 peptide bound weakly (K_d of 28.9 ± 1.1 μM). These affinities differ slightly from those determined earlier as discussed in the Materials and methods section, but are generally comparable (Guettler *et al*, 2008).

Loss-of-contact alanine substitutions of both helix α1 hydrophobic residues (α1^{AA} mutations), which contact the hydrophobic cleft of actin, virtually abolished detectable interaction with actin for all three RPEL peptides (Figure 3A). A similar result was observed when loss-of-contact alanine substitutions were introduced at hydrophobic residues within helix α2 and its C-cap sequence (α2^{AAA} mutations). This region makes hydrophobic contacts with the subdomain 3 ledge. α2^{AAA} mutations within RPEL1^{MAL} greatly reduced binding but nonetheless binding was still detectable ($K_d = 24.0 \pm 1.5$ μM) (Figure 3A). Combination of both α1^{AA} and α2^{AAA} mutations eliminated measurable actin binding of all three RPEL peptides (data not shown). Mutations at the conserved RPEL arginine and proline residues had context-specific effects, consistent with the distinct molecular interactions revealed in the structures. Mutation of the invariant RPEL arginine residue (RPEL1, R81; RPEL2, R125; RPEL3, R169) abolished measurable actin binding for RPEL2 and 3, but only reduced RPEL1 binding ($K_d = 17.7 \pm 2.4$ μM). The relatively small effect of the RPEL1 R81A mutation may reflect its failure to engage the F375^{actin} carboxylate, whereas the RPEL1^{MAL}-specific ionic interaction between R82 and E167^{actin} provides a compensatory effect. Consistent with this, mutation of both R81 and R82 of RPEL1^{MAL} to alanine effectively reduced the RPEL1-actin affinity ($K_d = 44.5 \pm 3.5$ μM), whereas the charge-reversal mutation RR81/82DD rendered binding undetectable.

The effect of alanine substitution of the conserved RPEL proline residue was also context-dependent. The RPEL2^{MAL} P126A mutant reduced affinity by 16-fold ($K_d = 30.8 \pm 2.3$ μM), consistent with an important role for the proline in maintaining the R-loop conformational integrity. In contrast, the analogous alanine substitution in RPEL1^{MAL}, which contains an arginine at this position, reduced affinity only 3.5-fold ($K_d = 3.7 \pm 0.5$ μM), whereas conversely, replacement of RPEL2^{MAL} P126 with arginine (analogous to RPEL1^{MAL}), also reduced binding affinity ($K_d = 19.5 \pm 3.1$ μM). The different contacts seen in the two structures are thus reflected in contrasting roles for the conserved RPEL R and P residues in RPEL1^{MAL} and RPEL2^{MAL}, respectively (see Discussion). Residues I122 and P126 of RPEL2^{MAL} are substituted by G and S, respectively, in the RPEL2 motif of myocardin (Figure 1A). These substitutions eliminate crucial G-actin contacts and are likely to account for the weak actin affinity exhibited by myocardin (Guettler *et al*, 2008). Alanine substitution at the conserved RPEL glutamate, which does not make direct contact with actin, had only a small effect on RPEL1^{MAL}:G-actin binding affinity (E86A, $K_d = 2.7 \pm 0.4$ μM), and did not affect RPEL2^{MAL}:G-actin interaction (E130A, $K_d = 1.9 \pm 0.2$ μM). The conservation of this residue among the family of RPEL motifs may reflect an additional conserved role unrelated to actin binding (see Discussion).

RPEL3^{MAL} retains all the equivalent residues to RPEL2^{MAL} that make direct interaction with actin, yet its affinity for actin is an order of magnitude lower than that of either RPEL1^{MAL} or RPEL2^{MAL} (Guettler *et al*, 2008). We hypothesised that non-consensus residues might be impairing RPEL3 binding to actin. Mapping the MAL RPEL3 sequence onto the RPEL1/RPEL2 structures identified that G171 immediately before helix α2^{RPEL3} could introduce considerable flexibility into the R-loop. More importantly, a proline residue at position 172 has no main chain amide available to hydrogen bond to the Y169^{actin} hydroxyl group. To test this hypothesis, we generated an 'RPEL2-like' RPEL3^{MAL} peptide by replacing RPEL3 G171/P172 by the corresponding residues from RPEL2^{MAL}, E and R. This substitution improved actin-binding affinity almost six-fold, to 4.8 ± 0.1 μM, compared with the wild-type RPEL3^{MAL} peptide, with actin binding remaining dependent on hydrophobic contacts between α2^{RPEL3} and the subdomain 3 ledge contact (Figure 3A).

Integrity of RPEL:G-actin contacts is required for MAL regulation

We observed earlier that mutations of the conserved core arginines, which lower RPEL^{MAL}:G-actin affinity, result in partial or complete nuclear accumulation of MAL protein in serum-starved cells, potentiate its transcriptional activity and uncouple its activation from Rho signalling (Guettler *et al*, 2008). We therefore tested whether the structure-based mutations that disrupt actin binding have a similar effect on MAL function *in vivo*. The loss-of-hydrophobic-contact mutations in helix α1, helix α2 and the flanking C-cap (α1^{AA} and α2^{AAA}) were introduced into full-length MAL (Figure 3B), and the mutant proteins were expressed by transient transfection in NIH3T3 cells. Activity was monitored by assessment of the

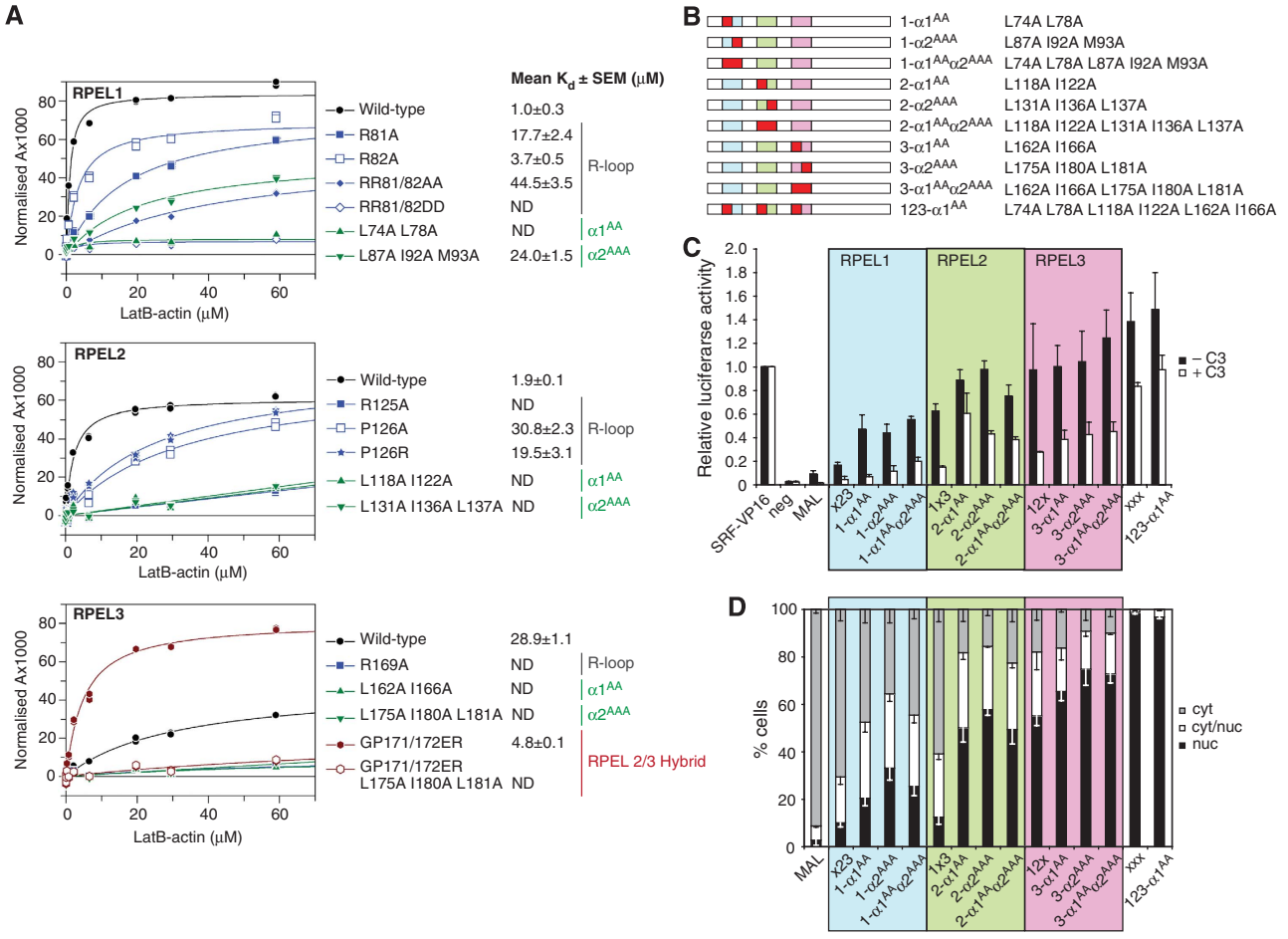

Figure 3 *In vitro* and *in vivo* validation of the RPEL1^{MAL} and RPEL2^{MAL} structures. (**A**) Fluorescence anisotropy assay for characterisation of the RPEL^{MAL}:G-actin interaction. Anisotropies of FITC-conjugated 32 amino-acid RPEL peptides at a concentration of 0.5 μM were measured over a range of LatB–actin concentrations. Anisotropy values were normalised by subtracting the anisotropy obtained in the absence of LatB–actin from all anisotropies for each peptide and multiplied by 1000. Graphs correspond to one of three experiments done in duplicate. Dissociation constants (K_d) for RPEL^{MAL}:G-actin interactions were calculated by nonlinear regression from each duplicate after normalisation using GraFit software (see Materials and methods). K_d values shown are means from three independent experiments with s.e.m. (**B**) Schematic representation of N-terminal MAL mutations used for luciferase reporter assays and immunofluorescence. The mutated region is shown in red. (**C**) SRF reporter activation by structure-derived MAL point mutants. The indicated MAL derivatives were expressed with and without C3 transferase coexpression in serum-starved NIH3T3 cells. Reporter activation was normalised to reporter activation conferred by SRF-VP16 or SRF-VP16 plus C3 transferase. x23, 1x3, 12x and xxx refer to MAL derivatives described earlier (Guettler *et al*, 2008): x23, R81A; 1x3, R125A; 12x, R169A; xxx, R81A R125A R169A. Data from three independent experiments are shown. Error bars, s.e.m. (**D**) Subcellular localisation of structure-derived MAL point mutants. The localisation of the indicated constructs was scored as predominantly nuclear (nuc), comparable intensity in nucleus and cytoplasm (nuc/cyt) or predominantly cytoplasmic (cyt) in 100 serum-starved cells. Mutants are described in (B, C). Data from three independent experiments are shown. Error bars, s.e.m.

proteins' subcellular localisation (Figure 3D) and by their ability to activate a co-transfected reporter gene for their transcription factor target SRF (Figure 3C and D).

Alanine substitutions at each core RPEL arginine substantially increased MAL nuclear localisation and SRF reporter activity, with mutations in RPEL1^{MAL} having a lesser effect than those in the other motifs, as reported previously (Guettler *et al*, 2008). Similar results were obtained on introduction of the α1^{AA} and α2^{AAA} substitutions into individual RPEL motifs. The α1^{AA} and α2^{AAA} mutant derivatives of MAL all activated the SRF reporter more strongly than wild-type MAL. Mutations in RPEL1^{MAL} were again less effective than those in the other RPEL motifs, although the RPEL1^{MAL} α1^{AA} and α2^{AAA} mutants were somewhat more active than the RPEL1^{MAL} R81A (x23) mutant. All the mutants exhibited a decreased dependence on functional Rho, with the combined introduction of the α1^{AA} mutation into all three repeats having the largest effect. Consistent with their increased activity in the reporter assay, each mutant exhibited substantially increased nuclear localisation. Taken together with the fluorescence anisotropy data, these results support the view that binding of actin to MAL is required to maintain its cytoplasmic localisation and suppress its activity as a transcriptional coactivator.

Discussion

Implications for RPEL^{MAL}:G-actin interactions and regulation of myocardin family SRF coactivators

Here, we describe in atomic detail how G-actin binds individual RPEL peptides from the MAL N-terminal regulatory domain and the structural fold adopted by an RPEL motif. The structures demonstrate that virtually all sequence conservation of the RPEL motif reflects its function as an actin-binding element. Structure-directed functional studies show that authentic MAL regulation requires that each of the three

RPEL motifs in the N-terminal regulatory domain be competent to bind G-actin. Together with our previous demonstration that signalling induces changes in MAL-actin interaction *in vivo* (Vartiainen *et al*, 2007), our data are consistent with a model in which alterations to actin loading onto the regulatory domain control MAL nuclear accumulation.

Actin binding is required for Crm1-dependent MAL nuclear export (Vartiainen *et al*, 2007) and is also likely to inhibit activity of a putative nuclear import signal within the RPEL2–RPEL3 linker (Vartiainen *et al*, 2007; Guettler *et al*, 2008). It is thus likely that different actin-bound states of the regulatory domain will exhibit different interactions with import and export factors. We identified earlier a stable 3:1 actin–MAL complex in gel filtration experiments (Vartiainen *et al*, 2007). This complex can effectively sequester actin from polymerisation, so the arrangement of the actin molecules in it must differ from that occurring within the actin filament (Posern *et al*, 2004). The relevance of this complex to MAL regulation, in terms of its competence to bind import factors or to recruit Crm1, remains unclear. Although the existence of the 3:1 actin–MAL complex is consistent with each RPEL engaging one actin molecule in the manner described in this study, this awaits direct confirmation. Our current work is focused on elucidation of the structure of the 3:1 actin–MAL complex.

Several considerations suggest that in the context of the MAL N-terminal regulatory domain the RPEL motifs do not function independently in a 'beads-on-a-string' manner. First, the high apparent affinity of the intact regulatory domain for actin compared with individual RPEL peptides suggests that cooperative actin–actin interactions may facilitate complex formation. Second, the non-canonical RPEL1 motif, and its distinct mode of actin binding, has been selected throughout metazoan evolution, as have the sequences responsible for the low affinity of the RPEL3 motif, suggesting the motifs have distinct functional roles. Third, comparative studies of MAL and its constitutively nuclear relative myocardin suggest that actin-regulated nuclear accumulation appears determined by the RPEL1–RPEL2 unit, RPEL3 being interchangeable (Vartiainen *et al*, 2007; Guettler *et al*, 2008). It will be interesting to examine whether RPEL3 loads actin last in an ordered assembly of multiple actin molecules onto the triple RPEL repeat region of MAL, and the potential functional significance of this for MAL cytoplasmic–nuclear shuttling.

In addition to controlling nuclear accumulation of MAL, actin binding also appears to repress the ability of nuclear MAL to activate transcription through SRF (Vartiainen *et al*, 2007; Guettler *et al*, 2008). At this level, MAL-bound actin may modulate the formation of ternary complexes of MAL, SRF and DNA, recruit transcriptional repressors or interfere with the formation of active transcription complexes.

The RPEL motif binds G-actin similarly to DBP

To understand how MAL is able to compete with other actin-binding proteins, including the highly abundant G-actin-buffering proteins profilin and thymosin β4 (Pollard and Borisy, 2003), we compared our RPEL peptide:G-actin structures with other actin-binding protein structures. This analysis showed that 'cleft-and-ledge' contacts from RPEL1 and 2 are strikingly similar to those made by vitamin D-binding protein (DBP), a large multi-domain actin-sequestering protein quite unrelated to the RPEL motif (Otterbein *et al*, 2002; Verboven *et al*, 2003) (Figure 4A). DBP uses two helices, structurally equivalent to those of RPEL1/2, to engage both the actin subdomain 1–3 hydrophobic cleft and the subdomain 3 ledge of actin (Figure 4A). This region of DBP and RPEL2^{MAL} superposes with an r.m.s. difference of 1.5 Å over 17 C-alpha atoms. The DBP helices are non-contiguous, however, being separated by over 100 amino acids in the primary sequence, and DBP therefore has no equivalent of the RPEL R-loop (Figure 4A). At least five structurally equivalent residues are shared by the RPEL motif and DBP. These include L184^{DBP} and L188^{DBP} (from helix α1); K191^{DBP}, which hydrogen bonds to E167^{actin} main chain (equivalent to R81/R125 of RPEL1/2); V294^{DBP} and F298^{DBP}, which contact the subdomain 3 ledge (Figure 4A, DBP residue numbers are taken from 1MA9 coordinates). The latter residue resides within a lengthened helix, which replaces the C-cap attached to the α2^{RPEL}, but has an analogous function to α2^{RPEL} C-cap residues I92/I136, which contact the subdomain 3 ledge. The unexpected similarity of actin contacts between RPEL and DBP raises the possibility that other cleft-and-ledge actin-binding proteins may yet be found.

An extended family of G-actin cleft-binding proteins

Similar to DBP and gelsolin, RPEL1 and RPEL2 of the MRTFs contain a helix that binds in the forward direction of the hydrophobic cleft in actin, a frequently used site for actin-binding proteins (McLaughlin *et al*, 1993; Robinson *et al*, 1999; Otterbein *et al*, 2002; Verboven *et al*, 2003; Burtnick *et al*, 2004; Paavilainen *et al*, 2008) (Figure 4B and C). 'Forward' is defined as the peptide ligand (N→C) running front-to-back in the conventional actin view (Dominguez, 2004) (Figure 1B). The unexpected similarity between RPEL and DBP actin contacts close to the subdomain 3 ledge (Figure 4A) prompted us to perform structure-based sequence alignments with other actin cleft-binding proteins to examine common structural features. Previous analysis identified three hydrophobic residues (designated A, B and C herein) that are present in most actin cleft-binding proteins (Dominguez, 2004) (Figures 4C and 5). Inclusion of RPEL and DBP contacts with actin identified an additional, highly conserved interaction involving a basic residue (designated D; see Figure 5), which was not explicitly described earlier as being conserved in both forward and reverse orientations. Residues A and D are present independently of the orientation of the cleft-binding helix, and they superpose well between the different structures (Figure 4C). There is more variability in the interactions made by residues B and C: for example, the hydrophobic residue C in the RPEL^{MAL} α1 and DBP helices is oriented towards the cleft floor rather than the side of the cleft. This positions residue B, which is in some instances a lysine residue, outside the cleft on the subdomain 3 surface but still able to contribute hydrophobic contacts via the aliphatic portion of its side chain (Figure 4C; see Supplementary Figure S2A).

In summary, our structural analysis provides the first detailed picture of how an RPEL peptide binds to G-actin and suggests functionally important differences between each MAL RPEL motif. To understand how MAL is regulated by higher order RPEL:G-actin assemblies, future experiments will concentrate on G-actin complexes with an intact triple RPEL domain from MAL.

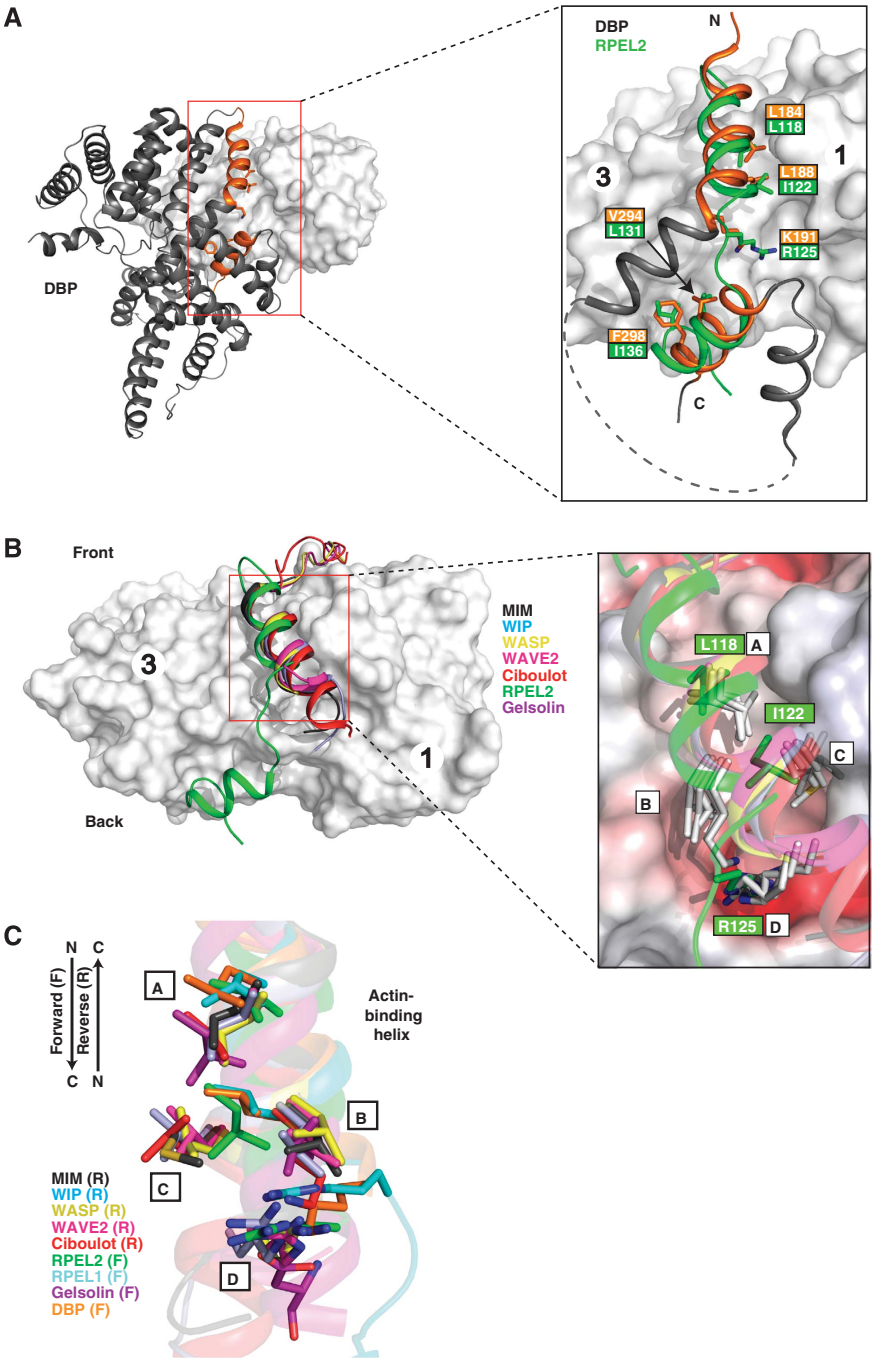

Figure 4 Structural comparison with known G-actin-binding proteins. (**A**) Left: the DBP:G-actin complex structure (PDB code 1MA9, actin as a white surface, DBP as grey cartoon ribbon). DBP helices that interact with the actin hydrophobic cleft and subdomain 3 ledge are shown in orange. Right: close-up of the actin hydrophobic cleft showing the binding interface of DBP and RPEL2^{MAL} superposed onto their respective G-actin partners. RPEL2^{MAL} is shown in green. DBP residue numbering is taken from the 1MA9 coordinates. (**B**) Left: bottom view of superposed WH2 motif containing proteins together with RPEL2^{MAL} bound to G-actin. MIM, black (PDB code 2D1K); WIP, marine blue (2A41); WASP, yellow (2A3Z); WAVE2, pink (2A40); Ciboulot, red (1SQK); RPEL2^{MAL} (green) gelsolin, purple (1EQY). Right: close up of the left-hand panel showing the side chains at the four conserved positions (A–D) together with an electrostatic surface of actin (red indicating acidic regions). The RPEL2^{MAL} α1 helix and its residue numbers are shown in green. (**C**) Structural alignment of helices equivalent to RPEL helix α1 from various G-actin-binding proteins. The four equivalent key residues common to these actin-binding proteins are displayed as sticks. The orientation of each helix is indicated in parentheses; R, reverse and F, forward.

Materials and methods

Plasmids

Sequences encoding mouse MAL RPEL peptides (see GST pull-down assays) were inserted into a vector derived from pET-41a(+) (Novagen; described in Vartiainen *et al*, 2007) for bacterial expression of GST–$(His)_6$–S-tag fusions (Guettler *et al*, 2008). Mammalian expression constructs for wild-type mouse MAL(fl)-HA_2 and human FLAG-β-actin and their mutant derivatives were based on pEF (Sotiropoulos *et al*, 1999; Miralles *et al*, 2003). SRF-VP16, C3 transferase and luciferase reporter plasmids were described earlier (Sotiropoulos *et al*, 1999; Geneste *et al*, 2002).

Proteins and peptides

Actin was prepared from rabbit skeletal muscle as described earlier (Feuer *et al*, 1948; Spudich and Watt, 1971). Peptides (both

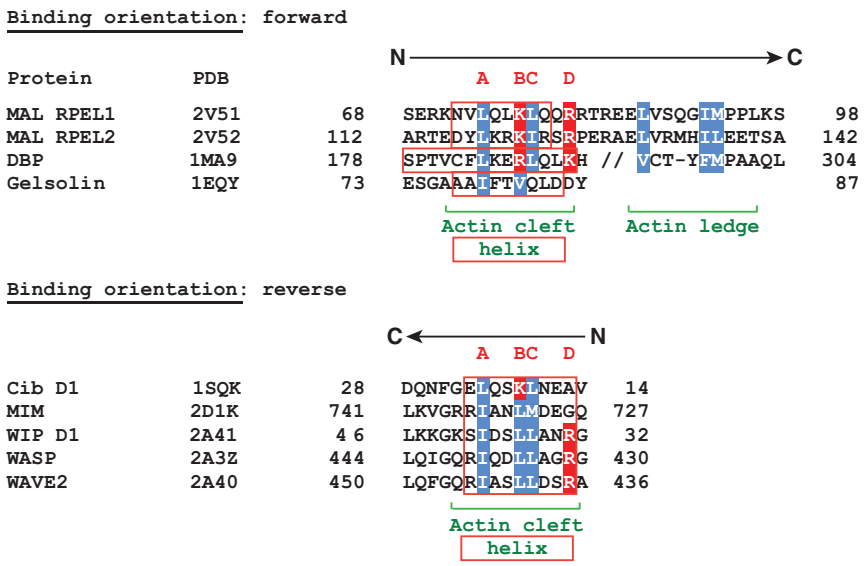

Figure 5 Structure-based sequence alignment of G-actin-binding proteins engaging the subdomain 1–3 hydrophobic cleft. The alignment is subdivided according to forward and reverse orientations of the actin-binding α-helix. Red boxes indicate experimentally observed helical regions. Cleft-binding residues A, B, C and D are highlighted as well as the three actin ledge-binding residues. Residue numbering for gelsolin and DBP are taken from the PDB coodinate files indicated and can be interconverted to full length sequence numbering by addition of 51 or 16 residues respectively.

unlabelled and N-terminally FITC-conjugated) corresponding to the three RPEL motifs of MAL were synthesised and HPLC-purified by the Cancer Research UK Protein and Peptide Chemistry Laboratory ($RPEL1^{MAL}$: MAL_{67-98}; $RPEL2^{MAL}$: $MAL_{111-142}$ and $RPEL3^{MAL}$: $MAL_{155-186}$). During the course of these studies, we discovered that the RPEL peptides exhibit varying degrees of methionine oxidation on storage and therefore we subjected all peptides to reduction and re-purification before analysis. Absorption of unlabelled peptides was measured at 215 nm (peptide bond) in an Agilent 8453 UV/Vis spectrophotometer and concentrations were calculated using $\varepsilon_{215} = 1000\ M^{-1}\ cm^{-1}$ per peptide bond. Absorption of FITC-conjugated peptides was measured at 492 nm (FITC) in a NanoDrop spectrophotometer (NanoTechnologies) using $\varepsilon_{492} = 83\,000\ M^{-1}\ cm^{-1}$.

Preparation of LatB–actin

We used LatB to block actin polymerisation, as successfully used in earlier crystallographic studies of actin (Morton *et al*, 2000; Hertzog *et al*, 2004). Briefly, rabbit skeletal muscle actin was dialysed into Mg^{2+}–G-buffer (2 mM Tris–HCl pH 8.0, 0.3 mM $MgCl_2$, 0.2 mM EGTA, 0.2 mM ATP and 0.5 mM DTT) and co-incubated overnight at 4°C with a 10-fold molar excess of LatB (Calbiochem), added from a 50 mM stock in DMSO. Un-complexed actin was polymerised for 1 h at 4°C on addition of 20 × initiation buffer (2 M NaCl, 60 mM $MgCl_2$ and 10 mM ATP). Actin filaments and insoluble material were removed by ultracentrifugation at 200 000 *g* for 15 min at 4°C. For crystallisation complex preparation, LatB–actin was concentrated using a 5000 MWCO Vivaspin 500 concentrator with a PES membrane, followed by another round of ultracentrifugation.

CD measurements and spectra deconvolution

CD spectra were recorded using an Aviv 202SF spectrophotometer in a 0.2 mm path length cell at 20°C. Data were recorded every 0.2 nm with a data acquisition time of 3 s in the range of 188–260 nm. Each peptide was dissolved in 10 mM Tris pH 8, 10 mM NaCl to a final concentration of 250 μM. Each spectrum was the average of three repeated scans. The composition of the secondary structure of each peptide was analysed from CD spectra using the DICHROWEB server (Whitmore and Wallace, 2004) and the algorithm CONTIN (van Stokkum *et al*, 1990).

Crystallisation, data collection and structure determination

RPEL:LatB–G-actin:ATP complexes were prepared at a molar ratio of 3:1 of RPEL:LatB-actin and at a final actin concentration of 12 mg/ml. The complexes were crystallised at 20°C using the sitting drop vapour diffusion method. Sitting drops of 1 μl consisted of a 1:1 (volume:volume) mixture of protein and a well solution containing 0.15 M potassium thiocyanate, 0.1 M sodium cacodylate pH 6.5, 15% polyethylene glycol 6000 for the RPEL1:LatB–actin complex, and 0.2 M sodium chloride, MES pH 6 and 20.5% polyethylene glycol 6000 for the RPEL2:LatB–actin complex. Crystals were flash-frozen in liquid nitrogen with 20% glycerol as a cryoprotectant.

X-ray datasets were collected at 100 K at the ID14-2 beamline of European Synchrotron Radiation Facility (Grenoble, France) for RPEL1 and at I03 beamline of Diamond Light Source (Oxford, UK). RPEL1:LatB–actin and RPEL2:LatB–actin structures were solved and refined at 2.35 and 1.45 Å, respectively. Data collection and refinement statistics are summarised in Supplementary Table 1. Both datasets were indexed with MOSFLM and scaled and merged with SCALA (CCP4 (Collaborative Computational Project N), 1994). Molecular replacement for each complex used a G-actin:Latrunculin A (Bubb *et al*, 2002) (PDB code: 1IJJ) search model in PHASER (McCoy *et al*, 2005). Refinement was carried out using REFMAC5 (Murshudov *et al*, 1997). Model building was performed with COOT (Emsley and Cowtan, 2004). The final $2mF_o-DF_c$ electron density map covering RPEL1 and RPEL2 peptides shows unambiguous density for residues 72–98 and 111–141, respectively. Model validation used PROCHECK (Laskowski *et al*, 1993) and figures were prepared using the graphics program PYMOL (http://www.pymol.org). Coordinates have been deposited within the PDB with codes 2V51 ($RPEL1^{MAL}$:G-actin) and 2V52 ($RPEL2^{MAL}$:G-actin).

Fluorescence anisotropy

Fluorescence anisotropy assays were performed essentially as described (Guettler *et al*, 2008). Binding experiments were carried out in 50 μl volumes in Mg^{2+}–F-buffer (2 mM Tris–HCl pH 8.0, 100 mM NaCl, 3 mM $MgCl_2$, 0.2 mM EGTA, 0.7 mM ATP and 2 mM DTT). FITC-conjugated peptides were used at 0.5 μM, whereas LatB–actin was added from 1 nM up to 59 μM. Plates were read in a Safire^2 microplate reader (Tecan) after 2 h co-incubation at room temperature to achieve binding equilibrium. The Safire^2 was used in fluorescence polarisation mode (excitation, 470 ± 20 nm; emission, 525 ± 20 nm; 10 reads; integration time, 40 μs) with the manufacturer's 'Magellan' software (version 5.03). Anisotropy (A) was calculated using the formula $A = (I_{parallel} - I_{perpendicular})/(I_{parallel} + 2I_{perpendicular})$, where $I_{parallel}$ and $I_{perpendicular}$ denote the fluorescence intensities parallel and perpendicular to the excitation

plane, respectively, and a G-factor of 1.2041. Anisotropy values were normalised by subtracting the anisotropy at [LatB–actin] = 0 from all anisotropies for each peptide and multiplied by 1000. Dissociation constants (K_d) were calculated by nonlinear regression in GraFit version 5.0.13 (Erithacus Software) using the following equation (Heyduk and Lee, 1990):

$$A = A_f + (A_b - A_f)\left(\frac{\left(\frac{1}{K_d}\right)[R_t] + \left(\frac{1}{K_d}\right)[L_t] + 1 - \sqrt{\left(\left(\frac{1}{K_d}\right)[R_t] + \left(\frac{1}{K_d}\right)[L_t] + 1\right)^2 - 4\left(\frac{1}{K_d}\right)^2 [R_t][L_t]}}{2\left(\frac{1}{K_d}\right)[R_t]}\right)$$

where A is the measured value of anisotropy; A_f and A_b are the anisotropy values corresponding to free and bound peptide, respectively; $[R_t]$ and $[L_t]$ are the total peptide ('receptor') and total LatB–actin ('ligand') concentrations, respectively; K_d is the dissociation constant. K_d values were derived from duplicate samples in three independent experiments with s.e.m.

GST pull-down assays

Approximately 10^7 NIH3T3 fibroblast cells on a 150-mm dish were transfected with 6 μg of pEF-FLAG-β-actin or its ΔF375 derivative using Lipofectamine reagent (Invitrogen). Cells were maintained in media containing 10% FCS for 1 day and serum-starved in media containing 0.5% FCS for another day. Glutathione-sepharose 4B (GE Healthcare) was saturated with recombinant GST (from empty vector) or GST fusion peptides (RPEL1: residues 67–98; RPEL2: 111–142; RPEL3: 155–187; MAL(fl) numbering) from *Escherichia coli* (Rosetta(DE3) pLysS; Novagen) lysates, washed and used as affinity resin in a binding reaction with total NIH3T3 cell extract, generated by lysis in binding buffer (50 mM Tris–HCl pH 8.0, 100 mM NaCl, 3 mM $MgCl_2$, 0.2 mM EGTA, 0.2 mM ATP, 1 mM DTT and protease inhibitors) through syringing and removal of insoluble material by centrifugation. An equivalent of a confluent 150-mm dish of NIH3T3 cells was used for four binding reactions. Binding was for 2 h in binding buffer at 4°C. The resin was washed three times in binding buffer without protease inhibitors and subjected to 4–12% SDS–PAGE and western blotting with detection of the FLAG epitope tag (M2 FLAG–HRP; Sigma) and total β-actin (AC-15; Sigma). The blot was stained with Ponceau S to reveal bait input.

Immunofluorescence microscopy

Immunofluorescence microscopy was performed as described earlier (Vartiainen *et al*, 2007; Guettler *et al*, 2008). NIH3T3 cells (150 000 cells per well in a six-well dish) were transfected with 100 ng of C-terminally HA-tagged MAL (MAL-HA_2) or the indicated MAL-HA_2 derivative. After transfection, cells were maintained in a medium containing 0.5% FCS for 20 h. Primary antibody was anti-HA (12CA5; Roche). The localisation of each MAL derivative was scored as predominantly nuclear, pancellular or predominantly cytoplasmic in 100 cells.

Luciferase reporter assay

Luciferase reporter assays were performed as described earlier (Vartiainen *et al*, 2007; Guettler *et al*, 2008). NIH3T3 cells (30 000 cells per well in a 24-well dish) were transfected with SRF reporter p3DA.luc (8 ng), reference reporter ptk-RL (20 ng) plus SRF-VP16 (40 ng) or MAL (10 ng) or MAL derivative (10 ng). Where indicated, C3 transferase was coexpressed (2 ng). After transfection, cells were maintained in a medium containing 0.5% FCS for 22 h. Firefly luciferase activity was measured and normalised to *Renilla* luciferase activity (Dual-Luciferase Reporter Assay System; Promega).

Supplementary data

Supplementary data are available at *The EMBO Journal* Online (http://www.embojournal.org).

Acknowledgements

We gratefully acknowledge access to the circular dichroism facilities within Professor John Ladbury's laboratory, Institute of Structural Molecular Biology, UCL/Birkbeck. We thank Nicola O'Reilly and the Cancer Research UK Protein and Peptide Chemistry Laboratory for expert peptide synthesis, members of the Treisman and McDonald laboratories for assistance and helpful discussions and Banafshe Larijani for access to the UV/Vis spectrophotometer. This study was supported by Cancer Research UK. SG, a fellow of the Studienstiftung des Deutschen Volkes, was supported by a Boehringer Ingelheim Fonds predoctoral scholarship. CAL is supported by a Marie Curie Intra European Fellowship within the 7th European Community Framework Programme.

References

Allen PB, Greenfield AT, Svenningsson P, Haspeslagh DC, Greengard P (2004) Phactrs 1–4: a family of protein phosphatase 1 and actin regulatory proteins. *Proc Natl Acad Sci USA* **101:** 7187–7192

Bubb MR, Govindasamy L, Yarmola EG, Vorobiev SM, Almo SC, Somasundaram T, Chapman MS, Agbandje-McKenna M, McKenna R (2002) Polylysine induces an antiparallel actin dimer that nucleates filament assembly: crystal structure at 3.5-Å resolution. *J Biol Chem* **277:** 20999–21006

Burtnick LD, Urosev D, Irobi E, Narayan K, Robinson RC (2004) Structure of the N-terminal half of gelsolin bound to actin: roles in severing, apoptosis and FAF. *EMBO J* **23:** 2713–2722

CCP4 (Collaborative Computational Project N) (1994) The CCP4 suite: programs for protein crystallography. *Acta Crystallogr D Biol Crystallogr* **50:** 760–763

Cen B, Selvaraj A, Burgess RC, Hitzler JK, Ma Z, Morris SW, Prywes R (2003) Megakaryoblastic leukemia 1, a potent transcriptional coactivator for serum response factor (SRF), is required for serum induction of SRF target genes. *Mol Cell Biol* **23:** 6597–6608

Chen M, Shen X (2007) Nuclear actin and actin-related proteins in chromatin dynamics. *Curr Opin Cell Biol* **19:** 326–330

Chereau D, Kerff F, Graceffa P, Grabarek Z, Langsetmo K, Dominguez R (2005) Actin-bound structures of Wiskott–Aldrich syndrome protein (WASP)-homology domain 2 and the implications for filament assembly. *Proc Natl Acad Sci USA* **102:** 16644–16649

Chhabra ES, Higgs HN (2007) The many faces of actin: matching assembly factors with cellular structures. *Nat Cell Biol* **9:** 1110–1121

Dominguez R (2004) Actin-binding proteins—a unifying hypothesis. *Trends Biochem Sci* **29:** 572–578

Emsley P, Cowtan K (2004) Coot: model-building tools for molecular graphics. *Acta Crystallogr D Biol Crystallogr* **60:** 2126–2132

Ermolenko DN, Thomas ST, Aurora R, Gronenborn AM, Makhatadze GI (2002) Hydrophobic interactions at the Ccap position of the C-capping motif of alpha-helices. *J Mol Biol* **322:** 123–135

Feuer G, Molnar F, Pettko E, Straub FB (1948) Studies on the composition and polymerization of actin. *Hung Acta Physiol* **1:** 150–163

Finn RD, Mistry J, Schuster-Bockler B, Griffiths-Jones S, Hollich V, Lassmann T, Moxon S, Marshall M, Khanna A, Durbin R, Eddy SR, Sonnhammer EL, Bateman A (2006) Pfam: clans, web tools and services. *Nucleic Acids Res* **34:** D247–D251

Geiger B, Bershadsky A (2001) Assembly and mechanosensory function of focal contacts. *Curr Opin Cell Biol* **13:** 584–592

Geneste O, Copeland JW, Treisman R (2002) LIM kinase and Diaphanous cooperate to regulate serum response factor and actin dynamics. *J Cell Biol* **157:** 831–838

Guettler S, Vartiainen MK, Miralles F, Larijani B, Treisman R (2008) RPEL motifs link the serum response factor cofactor MAL but not myocardin to Rho signaling via actin binding. *Mol Cell Biol* **28:** 732–742

Hertzog M, van Heijenoort C, Didry D, Gaudier M, Coutant J, Gigant B, Didelot G, Preat T, Knossow M, Guittet E, Carlier MF (2004) The beta-thymosin/WH2 domain; structural basis for the switch from inhibition to promotion of actin assembly. *Cell* **117:** 611–623

Heyduk T, Lee JC (1990) Application of fluorescence energy transfer and polarization to monitor Escherichia coli cAMP receptor protein and lac promoter interaction. *Proc Natl Acad Sci USA* **87:** 1744–1748

Holmes KC, Popp D, Gebhard W, Kabsch W (1990) Atomic model of the actin filament. *Nature* **347:** 44–49

Kabsch W, Mannherz HG, Suck D, Pai EF, Holmes KC (1990) Atomic structure of the actin:DNase I complex. *Nature* **347:** 37–44

Klenchin VA, King R, Tanaka J, Marriott G, Rayment I (2005) Structural basis of swinholide A binding to actin. *Chem Biol* **12:** 287–291

Laskowski RA, MacArthur MW, Moss DS, Thornton JM (1993) PROCHECK: a program to check the stereochemical quality of protein structures. *J Appl Crystallogr* **26:** 283–291

McCoy AJ, Grosse-Kunstleve RW, Storoni LC, Read RJ (2005) Likelihood-enhanced fast translation functions. *Acta Crystallogr D Biol Crystallogr* **61:** 458–464

McLaughlin PJ, Gooch JT, Mannherz HG, Weeds AG (1993) Structure of gelsolin segment 1–actin complex and the mechanism of filament severing. *Nature* **364:** 685–692

Miralles F, Posern G, Zaromytidou AI, Treisman R (2003) Actin dynamics control SRF activity by regulation of its coactivator MAL. *Cell* **113:** 329–342

Miralles F, Visa N (2006) Actin in transcription and transcription regulation. *Curr Opin Cell Biol* **18:** 261–266

Morton WM, Ayscough KR, McLaughlin PJ (2000) Latrunculin alters the actin–monomer subunit interface to prevent polymerization. *Nat Cell Biol* **2:** 376–378

Murshudov GN, Vagin AA, Dodson EJ (1997) Refinement of macromolecular structures by the maximum-likelihood method. *Acta Crystallogr D Biol Crystallogr* **53:** 240–255

Otterbein LR, Cosio C, Graceffa P, Dominguez R (2002) Crystal structures of the vitamin D-binding protein and its complex with actin: structural basis of the actin-scavenger system. *Proc Natl Acad Sci USA* **99:** 8003–8008

Otterbein LR, Graceffa P, Dominguez R (2001) The crystal structure of uncomplexed actin in the ADP state. *Science* **293:** 708–711

Paavilainen VO, Oksanen E, Goldman A, Lappalainen P (2008) Structure of the actin-depolymerizing factor homology domain in complex with actin. *J Cell Biol* **182:** 51–59

Pollard TD, Borisy GG (2003) Cellular motility driven by assembly and disassembly of actin filaments. *Cell* **112:** 453–465

Pollard TD (2007) Regulation of actin filament assembly by Arp2/3 complex and formins. *Annu Rev Biophys Biomol Struct* **36:** 451–477

Posern G, Miralles F, Guettler S, Treisman R (2004) Mutant actins that stabilise F-actin use distinct mechanisms to activate the SRF coactivator MAL. *EMBO J* **23:** 3973–3983

Revenu C, Athman R, Robine S, Louvard D (2004) The co-workers of actin filaments: from cell structures to signals. *Nat Rev Mol Cell Biol* **5:** 635–646

Robinson RC, Mejillano M, Le VP, Burtnick LD, Yin HL, Choe S (1999) Domain movement in gelsolin: a calcium-activated switch. *Science* **286:** 1939–1942

Sagara J, Higuchi T, Hattori Y, Moriya M, Sarvotham H, Shima H, Shirato H, Kikuchi K, Taniguchi S (2003) Scapinin, a putative protein phosphatase-1 regulatory subunit associated with the nuclear nonchromatin structure. *J Biol Chem* **278:** 45611–45619

Schuster-Bockler B, Schultz J, Rahmann S (2004) HMM logos for visualization of protein families. *BMC Bioinformatics* **5:** 7

Schutt CE, Myslik JC, Rozycki MD, Goonesekere NC, Lindberg U (1993) The structure of crystalline profilin-beta-actin. *Nature* **365:** 810–816

Sotiropoulos A, Gineitis D, Copeland J, Treisman R (1999) Signal-regulated activation of serum response factor is mediated by changes in actin dynamics. *Cell* **98:** 159–169

Spudich JA, Watt S (1971) The regulation of rabbit skeletal muscle contraction. I. Biochemical studies of the interaction of the tropomyosin–troponin complex with actin and the proteolytic fragments of myosin. *J Biol Chem* **246:** 4866–4871

Su Y, Kondrikov D, Block ER (2007) Beta-actin: a regulator of NOS-3. *Sci STKE* **2007:** pe52

van Stokkum IH, Spoelder HJ, Bloemendal M, van Grondelle R, Groen FC (1990) Estimation of protein secondary structure and error analysis from circular dichroism spectra. *Anal Biochem* **191:** 110–118

Vartiainen MK, Guettler S, Larijani B, Treisman R (2007) Nuclear actin regulates dynamic subcellular localization and activity of the SRF cofactor MAL. *Science* **316:** 1749–1752

Verboven C, Bogaerts I, Waelkens E, Rabijns A, Van Baelen H, Bouillon R, De Ranter C (2003) Actin-DBP: the perfect structural fit? *Acta Crystallogr D Biol Crystallogr* **59:** 263–273

Wang D, Chang PS, Wang Z, Sutherland L, Richardson JA, Small E, Krieg PA, Olson EN (2001) Activation of cardiac gene expression by myocardin, a transcriptional cofactor for serum response factor. *Cell* **105:** 851–862

Whitmore L, Wallace BA (2004) DICHROWEB, an online server for protein secondary structure analyses from circular dichroism spectroscopic data. *Nucleic Acids Res* **32:** W668–W673

